Simultaneous Achievement of High Performance and Low Sintering Temperature in Ultra-high Curie Temperature $La_2Ti_2O_7$ Ceramics by V_2O_5 Additive

Manjing Tang, Zhi Tan,* Jie Xing, Ning Chen, Hao Chen, Hongjiang Li, and Jianguo Zhu*

College of Materials Science and Engineering,

Sichuan University,

Chengdu 610064, China.

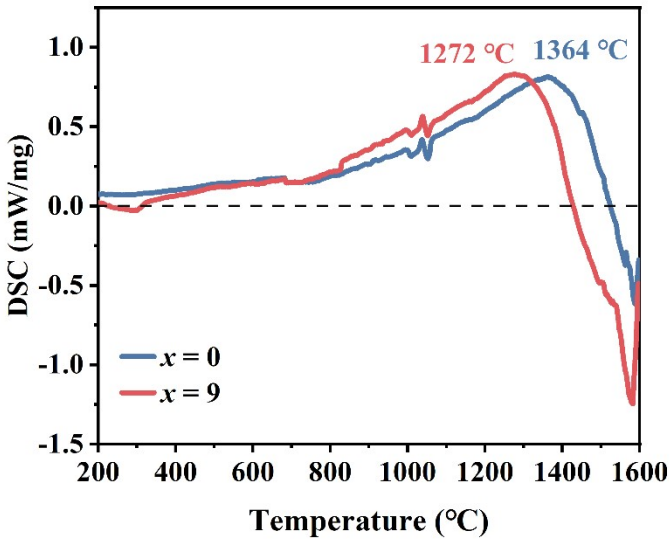

Fig. S1. DSC curves of LTO-*x*V ceramics (a) x =0 and (b) x = 9.

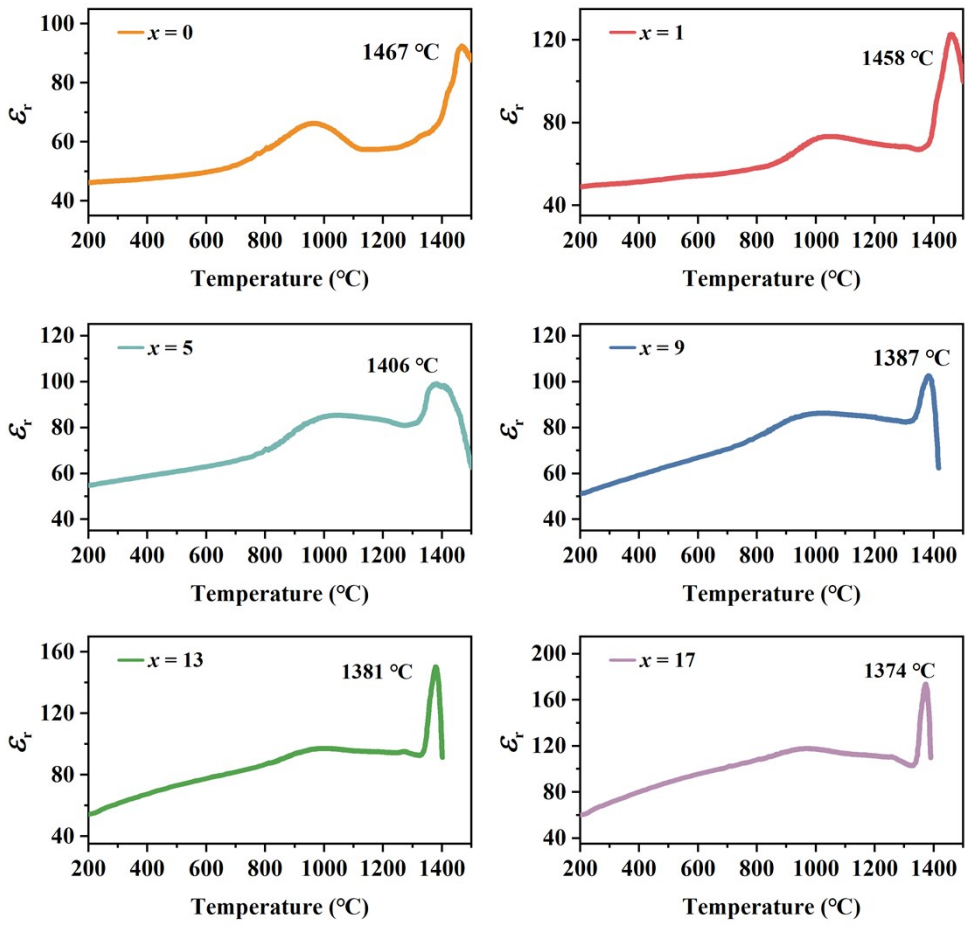

Fig. S2. The temperature dependence of relative dielectric permittivity of the LTO-*x*V ceramics at 1 MHz.

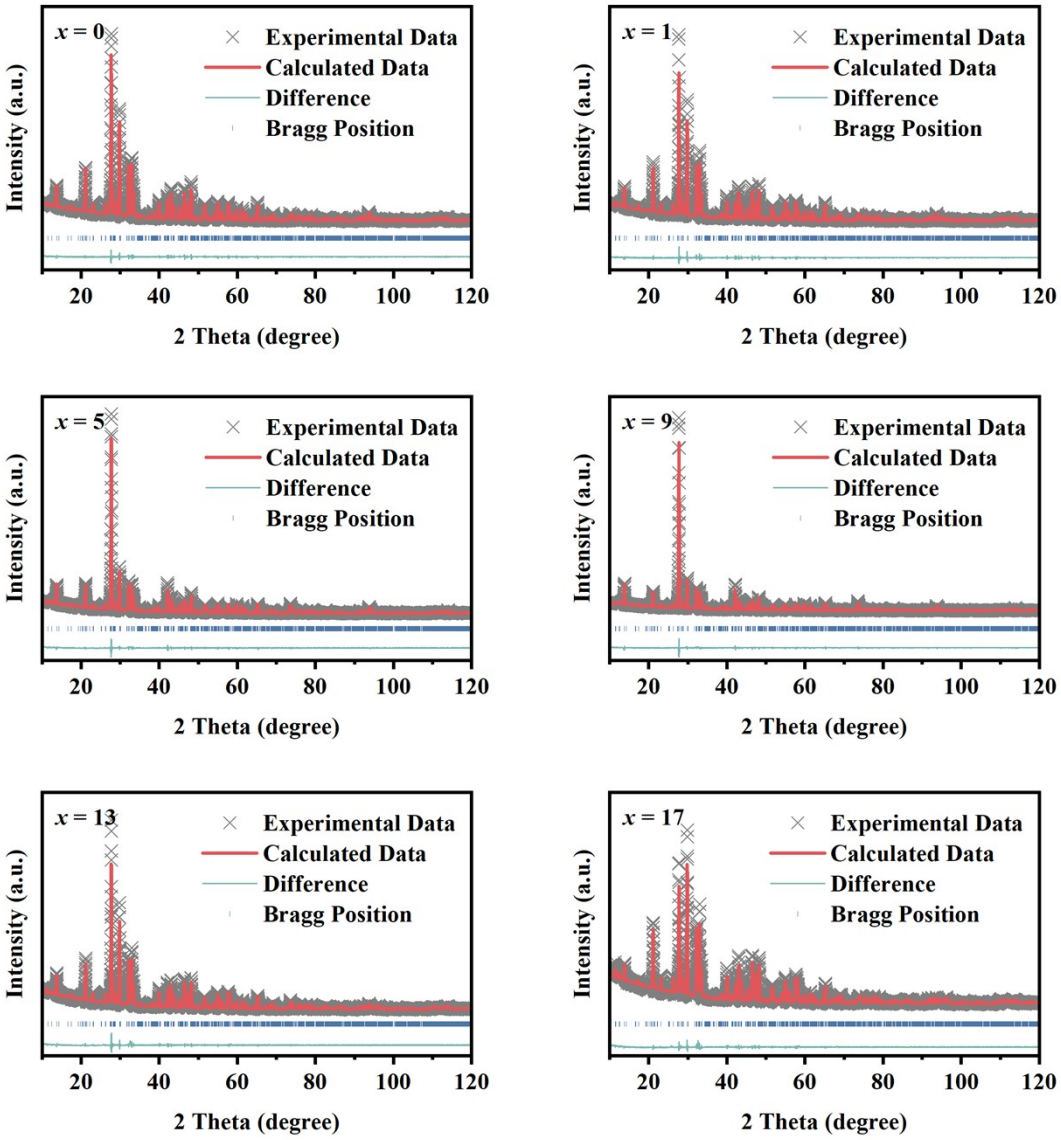

Fig. S3. Rietveld refinement plots of XRD patterns of the LTO-*x*V ceramic samples.

Table S1. The six major vibrational modes obtained according to the fitting results of LTO ceramics.

Raman shift (cm^{-1})	Band assignment	Peak
152	La-O	P_1
233	La-O	P_2
339	La-O	P_3
604	TiO_6	P_4
785	Ti-O stretching	P_5

808	Ti-O stretching	P_6

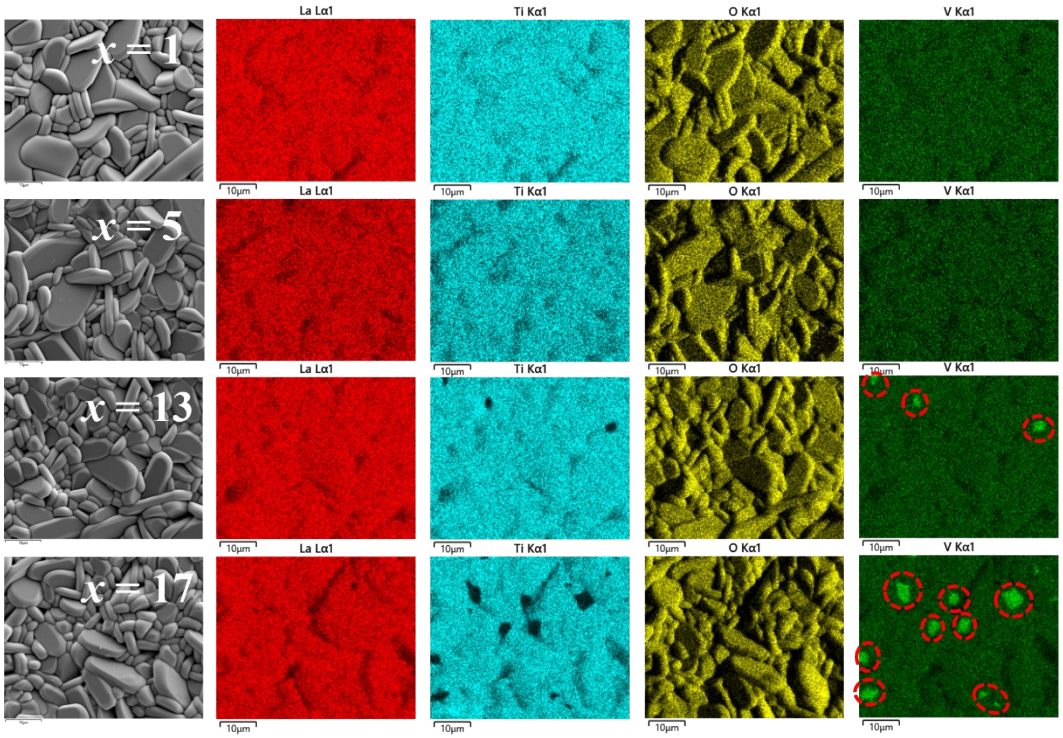

Fig. S4. SEM element mapping of the LTO-*x*V ceramic surface.

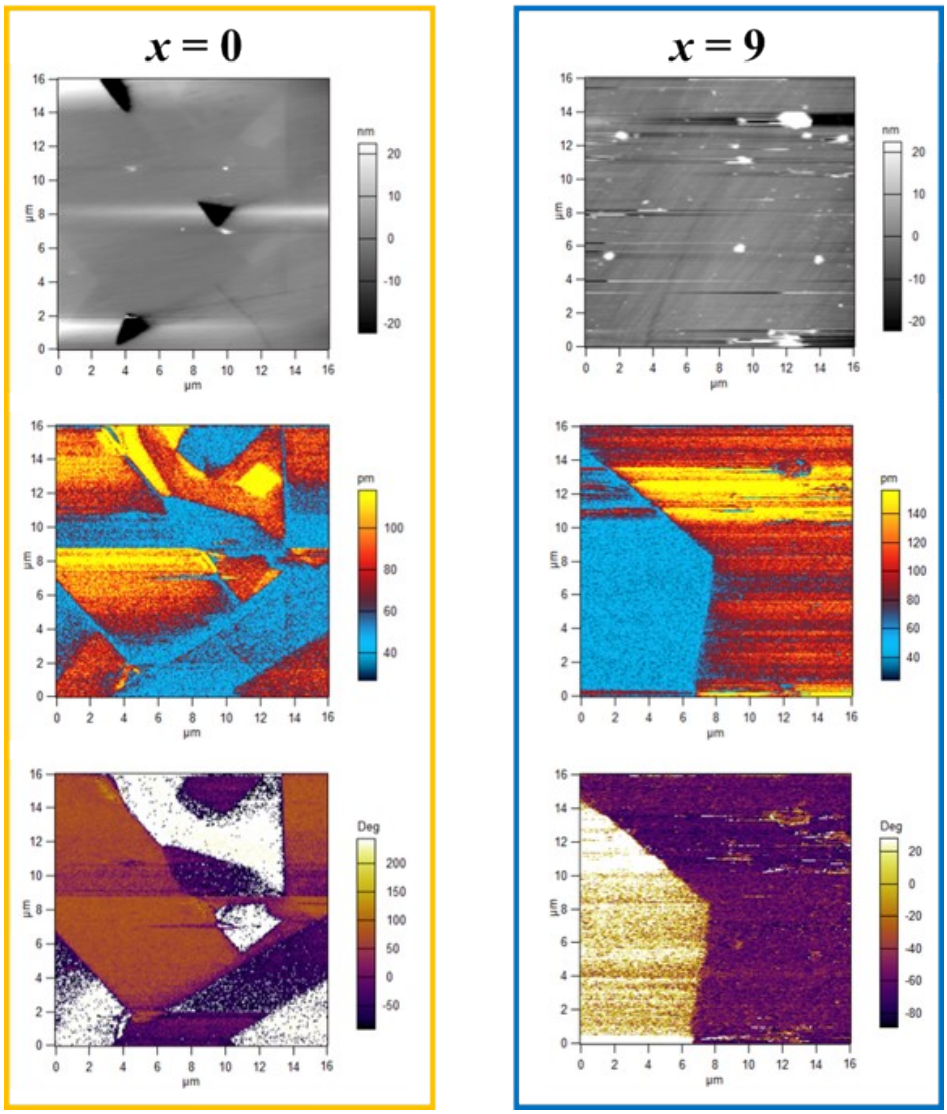

Fig. S5. PFM images of the LTO-*x*V ceramics with x =0 and x = 9 in a scanning region of 16 × 16 μm^2 at room temperature.

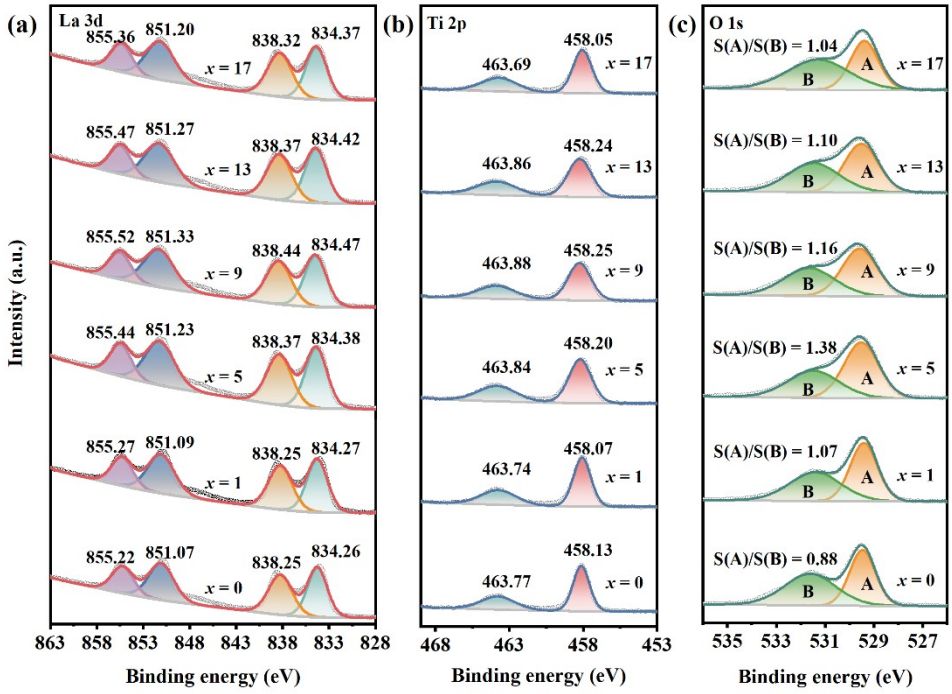

Fig. S6. High-resolution XPS spectra of (a) La 3d, (b) Ti 2p and (c) O 1s for the LTO-*x*V ceramics.

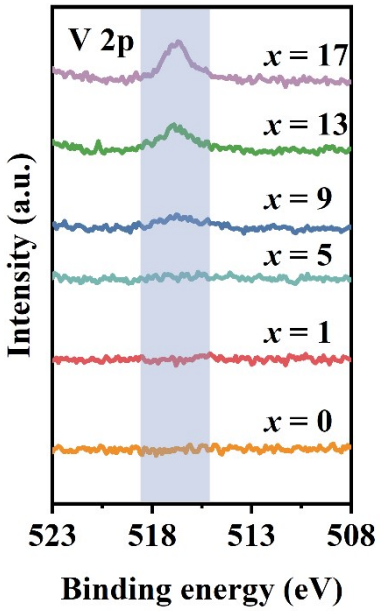

Fig. S7. High-resolution XPS spectra of V 2p for the LTO-*x*V ceramics.

The activation energy of conductivity was calculated by Arrhenius Equation:

$$\rho_{dc} = \rho_0 \exp\left(\frac{E_{cond}}{k_B T}\right)$$

where ρ_0 is the pre-exponent constant, E_{cond} is the activation energy of conductivity, k_B is the Boltzmann constant and T is the absolute temperature.

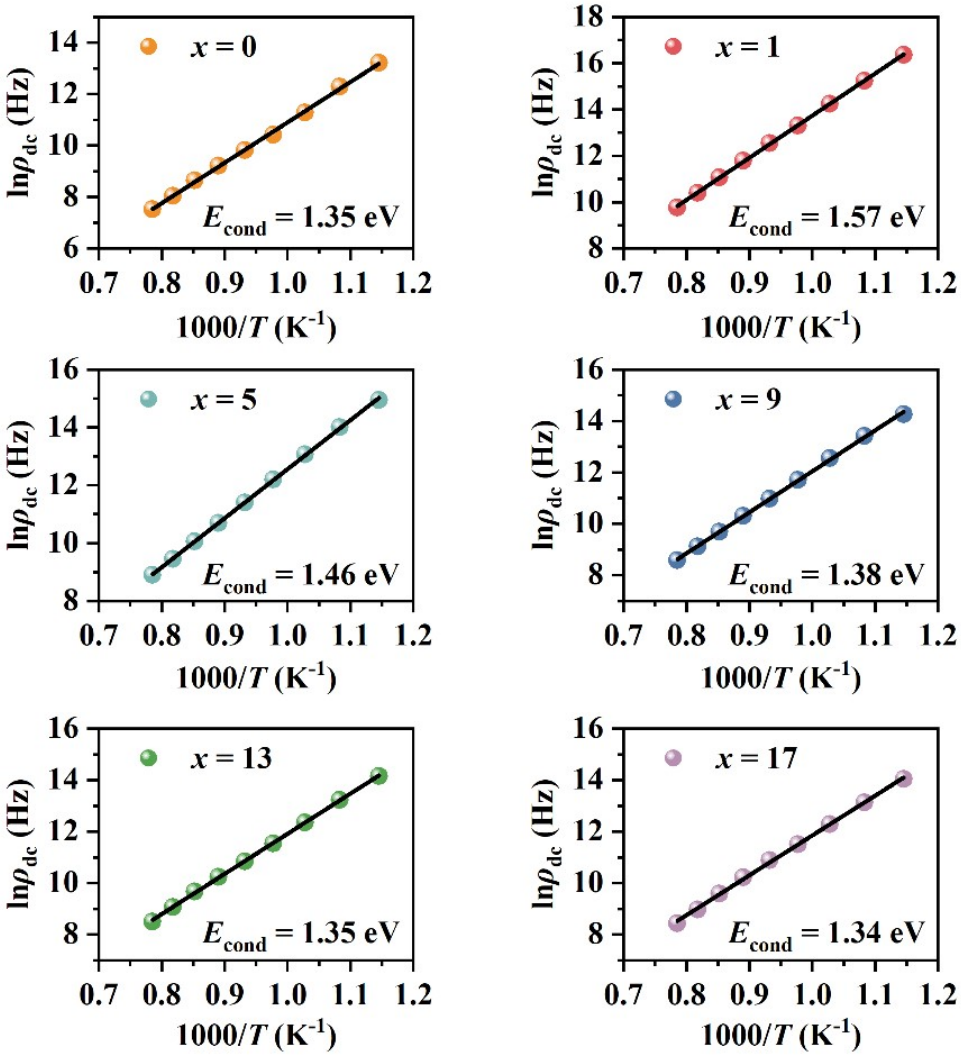

Fig. S8. The relationship between the temperature and ρ_{dc} fitted by the Arrhenius equation and the calculated E_{cond} of the LTO-xV ceramics.

The ideal Debye model assumes that a single relaxation time τ dominates the dielectric relaxation behavior of the material. In the Debye model, the relationship between relaxation time τ and the peak frequency f_{max} is $\tau = \frac{1}{2\pi f_{max}}$. With the addition of V_2O_5, the peak

frequency shifts from the high-frequency range to the low-frequency range, indicating an increase in relaxation time. The prolonged relaxation time indicates that charge carrier migration within the material has become more difficult, leading to reduced dielectric loss and enhanced insulation properties.

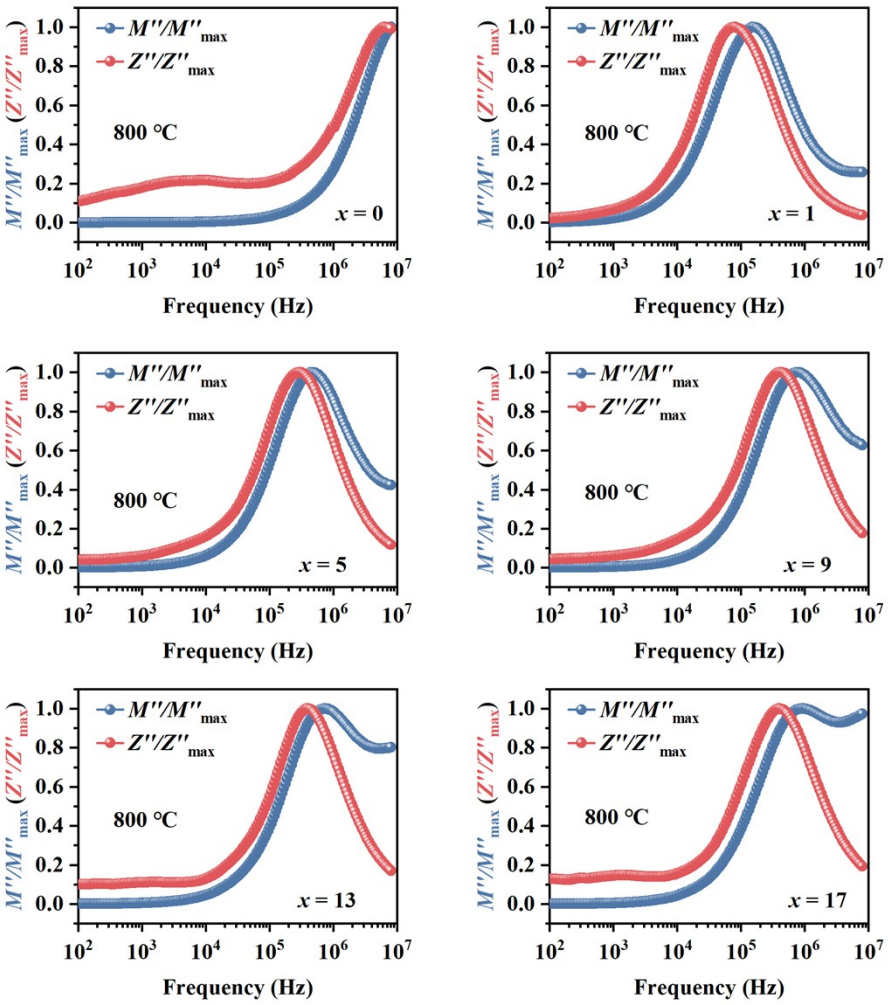

Fig. S9. The frequency dependence of Z''/Z''_{max} and M''/M''_{max} of the LTO-*x*V ceramics at 800 °C.

The Arrhenius equation was used to calculate the activation energy of the relaxation behavior for the LTO-*x*V ceramics. The impedance measurements were conducted over a frequency range of 100 Hz to 8 MHz and a temperature range of 600 °C to 1000 °C, with intervals of 50 °C. For the pristine sample $x = 0$, it was observed that the maximum normalized electric modulus (M'') values occurred at 8 MHz for temperatures above 800 °C. Consequently,

Arrhenius equation fitting was performed using the data at 600 °C, 650 °C, 700 °C, and 750 °C. For the remaining data, fitting was carried out within the temperature range of 600 °C to 850 °C.

The activation energy of the relaxation behavior was calculated by Arrhenius Equation:

$$f_p = f_0 \exp\left(-\frac{E_{relax}}{k_B T}\right)$$

where f_0 is attempt jump frequency, f_p is the frequency of M''_{max}, E_{relax} is the activation energy of relaxation behavior, k_B is the Boltzmann constant and T is the absolute temperature.

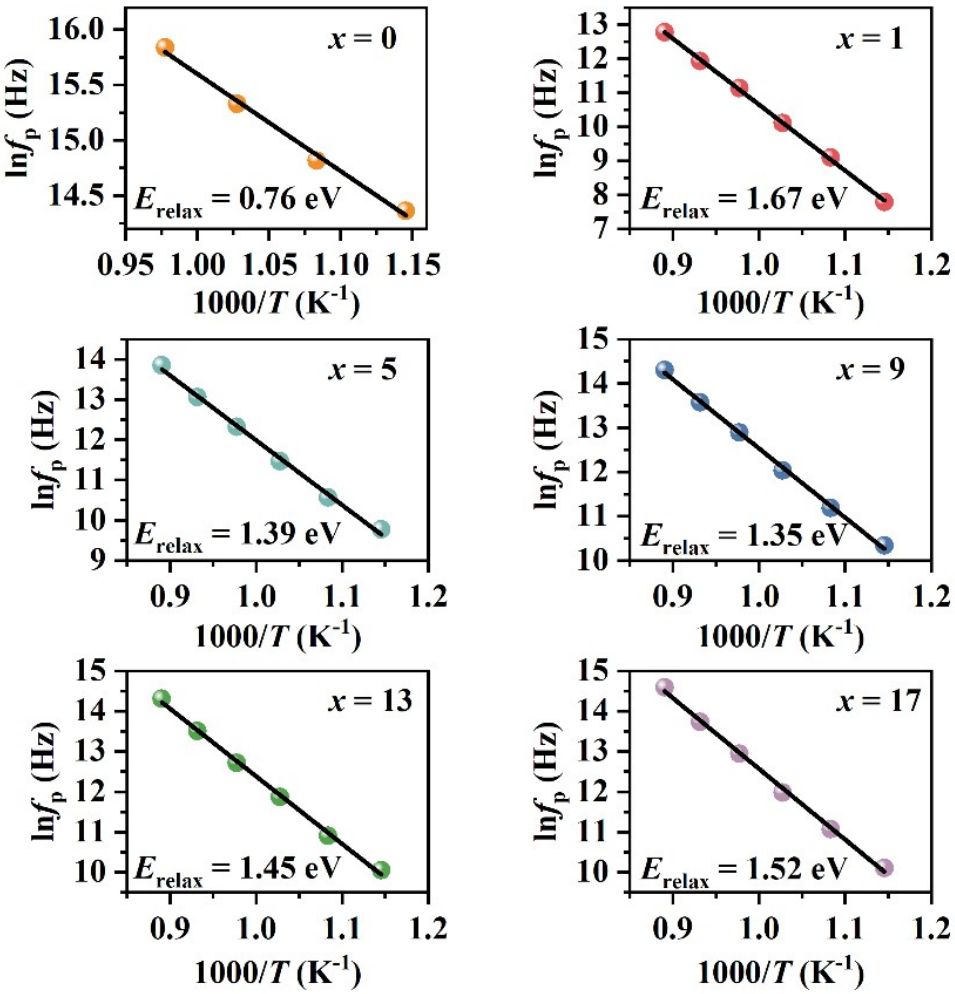

Fig. S10. The relationship between the temperature and f_p fitted by the Arrhenius equation and the calculated E_{relax} of the LTO-xV ceramics.